

## Article

# Synthesis of Cobalt Complex Containing *Trans*-Cinnamate and Its Electrocatalytic Activity for Oxygen Evolution Reaction

Jimin Lee <sup>1,†</sup>, Hyewon Shin <sup>1,†</sup>, Sunwoo Geum <sup>1</sup>, Sowon Lee <sup>1</sup>, Kang Min Ok <sup>2</sup> , Junghwan Do <sup>1,\*</sup>  
and Seong Jung Kwon <sup>1,\*</sup> 

<sup>1</sup> Department of Chemistry, Konkuk University, 120 Neungdong-ro, Gwangjin-gu, Seoul 05029, Republic of Korea

<sup>2</sup> Department of Chemistry, Sogang University, 35 Baekbeom-ro, Mapo-gu, Seoul 04107, Republic of Korea

\* Correspondence: junghwan@konkuk.ac.kr (J.D.); sjkwon@konkuk.ac.kr (S.J.K.); Tel.: +82-2-450-0429 (S.J.K.)

† These authors contributed equally to this work.

**Abstract:** There are many efforts reported on finding effective catalysts for oxygen evolution reactions (OERs), which are important reactions in the energy field. Coordination polymers, including metal–organic frameworks (MOFs), are attracting attention as electrocatalysts for OERs due to their versatility and modulating properties. A new cobalt complex containing *trans*-cinnamate and 2-aminopyridimidine ligands was synthesized using a hydrothermal method. The cobalt complex showed a 1D chain structure. The electrocatalytic activity and stability of the cobalt complex with or without an electrochemical supporter, such as reduced graphene oxide (rGO), OERs were investigated and compared with a metal oxide reference material. Due to the  $\pi$ -conjugated *trans*-cinnamate, which has electron flexibility near the Co centers, the catalyst/rGO composite showed significant catalytic activities, with an overpotential of 386 mV and a Tafel slope of 64 mV/dec.

**Keywords:** oxygen evolution reaction; electrocatalyst; coordination polymers; metal–organic frameworks; cobalt complex



**Citation:** Lee, J.; Shin, H.; Geum, S.; Lee, S.; Ok, K.M.; Do, J.; Kwon, S.J. Synthesis of Cobalt Complex Containing *Trans*-Cinnamate and Its Electrocatalytic Activity for Oxygen Evolution Reaction. *Catalysts* **2023**, *13*, 507. <https://doi.org/10.3390/catal13030507>

Academic Editors: Kyubock Lee and Min-Jae Kim

Received: 2 February 2023

Revised: 26 February 2023

Accepted: 26 February 2023

Published: 1 March 2023



**Copyright:** © 2023 by the authors. Licensee MDPI, Basel, Switzerland. This article is an open access article distributed under the terms and conditions of the Creative Commons Attribution (CC BY) license (<https://creativecommons.org/licenses/by/4.0/>).

## 1. Introduction

Research into new energy systems has garnered much attention over the past few decades due to the depletion of fossil fuels and the resulting environmental pollution. In this regard, oxygen evolution reactions (OERs) are important for efficient energy conversion and storage, especially in the case of fuel cells [1–5]. However, owing to the high overpotential for O–H bond cleavage and O–O bond formation, the kinetics of OERs are sluggish [6,7]. Therefore, the use of a catalyst is essential to reduce the massive energy consumption that would otherwise be needed.

The most representative electrocatalysts for OERs are noble metals, such as Ir and Ru, but they are expensive and in limited supply [8,9]. Contrarily, transition metal oxides are well-known electrocatalysts with a wide performance range due to the redox couples of their metal centers. In particular, non-noble metal oxides, such as Ni, Co, and Mn oxides, have been studied because of their low cost and high efficiency [10,11].

Coordination polymers, including metal–organic frameworks (MOFs), are also considered promising OER electrocatalysts. Their large surface areas, distinctively adjustable porous architectures, and electrical influence of the functional organic components on metal cores make MOFs beneficial [12,13].

Recently, we reported on the synthesis and electrocatalytic properties of the 3D porous cobalt cinnamate  $\text{Co}_7(\textit{trans}\text{-cinnamate})_{14}(\text{H}_2\text{O})_2$ , which showed superior electrocatalytic behavior, especially in the OERs of inorganic cobalt oxides [14,15]. Previous research revealed that the incorporation of the  $\pi$ -conjugated carboxylate *trans*-cinnamate, which can be easily separated from the cobalt cation due to the oxygen atoms in cobalt cinnamate having electron-poor environments compared to simple inorganic cobalt oxides, was responsible for the excellent OER electrocatalytic performance of cobalt cinnamate [16–18].

In this work, we presented another cobalt cinnamate complex that incorporates 2-aminopyrimidine. In this case, unique tetrameric  $\text{Co}_4$  units bridged by  $\text{H}_2\text{O}$  and *trans*-cinnamate anions are linked to each other through a 2-aminopyrimidine ligand, which completes the 1D chain structure. This cobalt complex incorporating  $\pi$ -conjugated *trans*-cinnamate and 2-aminopyrimidine was expected to exhibit similar electrical behaviors.

In addition, reduced graphene oxide (rGO) was employed as an electrochemical supporter for introducing a catalyst into an electrode surface to enhance the electrocatalytic performance by increasing the electrical contact between the electrode surface and the catalyst. Many previous studies have reported that the use of rGO as a supporter can provide a higher surface area and good electrical conductivity, enabling an efficient electrocatalyst reaction [19–21].

In this study, a new cobalt cinnamate complex was developed that incorporates 2-aminopyrimidine (catalyst **1**) as an electrocatalyst and rGO as an electrochemical supporter for OERs. The electrocatalytic performances of catalyst **1** with or without the rGO supporter were investigated using linear sweep voltammetry (LSV) and chronoamperometry (CA).

## 2. Results

Catalyst **1** was prepared by employing a hydrothermal method. By mixing  $\text{CoCl}_2 \cdot 6\text{H}_2\text{O}$ , 2-aminopyrimidine, and *trans*-cinnamic acid in water, we produced catalyst **1** in the form of red, polyhedral-shaped crystals. A powder X-ray diffraction (XRD) analysis confirmed the homogeneity and purity of the bulk products (FigureS S1 and S2 in the Supporting Information, SI). The structure of **1** was composed of infinite neutral  $\text{Co}_2(\text{trans-cinnamate})_4(2\text{-aminopyrimidine})_2(\text{H}_2\text{O})$  chains. Heavily disordered lattice water molecules were located between the chains. There were two crystallographically distinct cobalt atoms. The Co(1) atom was coordinated by four *trans*-cinnamate ligands to form  $\text{CoO}_4$  in a square planar geometry in the range of 2.031(2)–2.133(2) Å. To complete the slightly distorted octahedral coordination of  $\text{CoNO}_4(\text{H}_2\text{O})_2$ , an additional water molecule was coordinated to Co at a distance of 2.207(2) and one nitrogen atom from 2-aminopyrimidine at a distance of 2.244(3) in the *trans* position. The coordination environment of the other Co(2) atom was very similar to that of Co(1), except that one of the *trans*-cinnamate ligands in the square plane was replaced by 2-aminopyrimidine (Figure 1a). The bond valence sum (BVS) calculations for Co(1) and Co(2) resulted in values of 1.95 and 1.85, respectively, indicating an oxidation state of +2.00 [22].

The Co octahedra formed dimeric units by sharing the coordinated water molecule and two *trans*-cinnamate ligands (Figure 1). The dimers were connected to each other by bridging two *trans*-cinnamate ligands to produce a tetrameric unit. As shown, there were five *trans*-cinnamate and three 2-aminopyrimidine ligands in the dimer, two of which were used to form dimers by connecting the Co(1) and Co(2) octahedra, and two other *trans*-cinnamate contributed to connecting the dimers to form tetramers. The other *trans*-cinnamate and one of the three 2-aminopyrimidine molecules remained terminal, and the other two 2-aminopyrimidines acted as bridging ligands connecting the dimers.

Overall, the  $\text{Co}_4(\text{trans-cinnamate})_8(2\text{-aminopyrimidine})_4(\text{H}_2\text{O})_2$  tetrameric units were alternately connected to each other by two 2-aminopyrimidine ligands to produce neutral  $\text{Co}_2(\text{trans-cinnamate})_4(2\text{-aminopyrimidine})_2(\text{H}_2\text{O})$  chains along the *a*-axis (Scheme 1; Figure 1b). The interchain packing of **1** is shown in Figure 1c. The closest interchain contact was found between the *trans*-cinnamate ligands ( $d(\text{C}11 \cdots \text{C}14) = 3.483(4)$  Å), forming a weak  $\pi$ – $\pi$  stacking. The next closest interchain contact was found between *trans*-cinnamate and 2-aminopyrimidine ( $d(\text{C}6 \cdots \text{C}13) = 3.490(4)$  Å). This implied that the van der Waals interactions were dominant and the  $\pi$ – $\pi$  stacking between the chains was weak.

The electrocatalytic properties of catalyst **1** with or without the rGO supporter were investigated with respect to OERs. The linear sweep voltammograms (LSVs) of catalyst **1** and the reference material-modified glassy carbon electrode (GCE) are shown in Figure 2a. The onset potentials of the electrocatalysts with rGO were ~40 to 60 mV less positive than those of the cases without rGO.

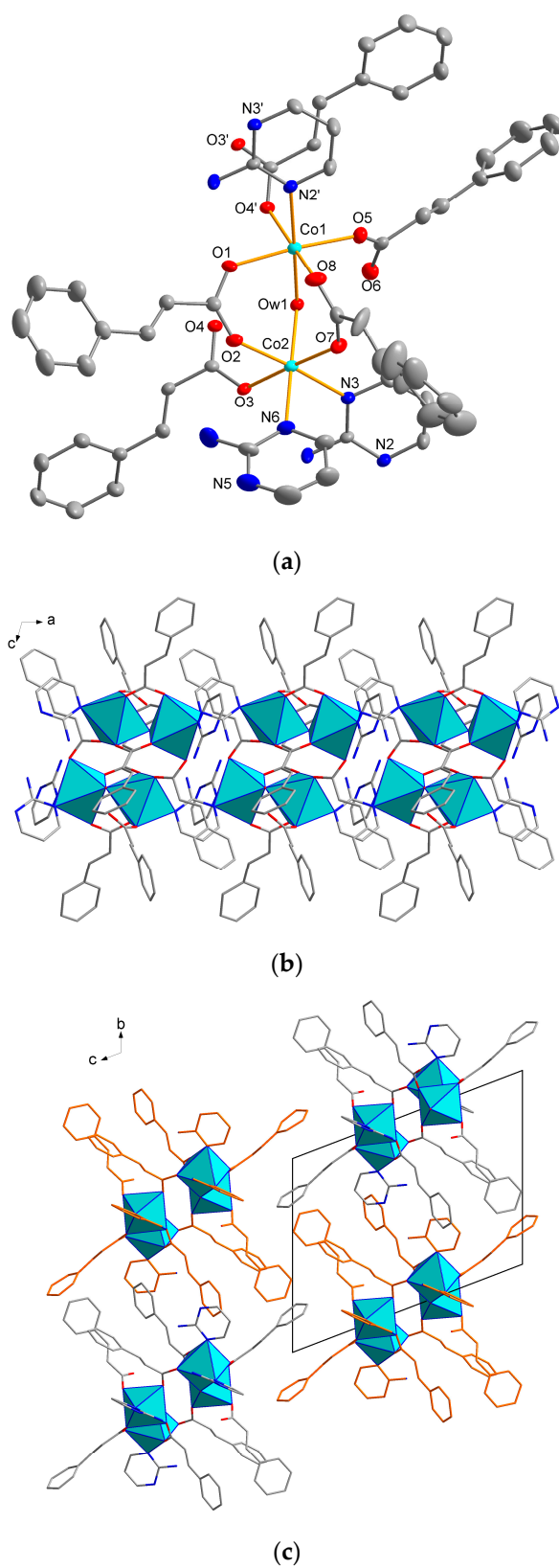
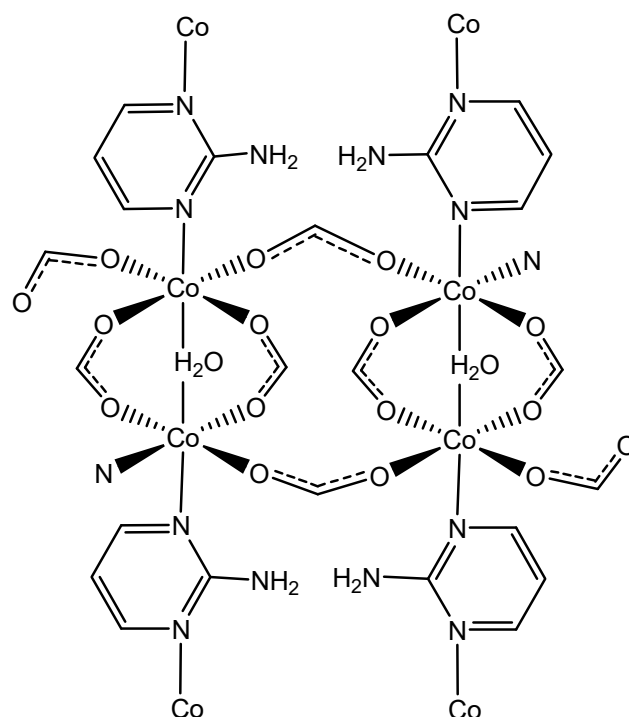


**Figure 1.** (a) Displacement ellipsoids of the molecular structure of **1**, drawn at a 30% probability level. The hydrogen atoms are omitted for clarity. The carbon, oxygen, nitrogen, and cobalt atoms are shown as gray, red, blue, and cyan spheres, respectively. (b) A chain of **1** is formed along the a-axis. The cyan polyhedra represent the cobalt atoms. (c) A view of the interlayer packing in **1**. Two bonding colors are shown to simply distinguish the different chains.



**Scheme 1.** Connectivity of Co and ligands (water, *trans*-cinnamate, and 2-aminopyrimidine) in forming chains. Only the carboxylate group in the *trans*-cinnamate and the N atom in the terminal 2-aminopyrimidine are shown for clarity.

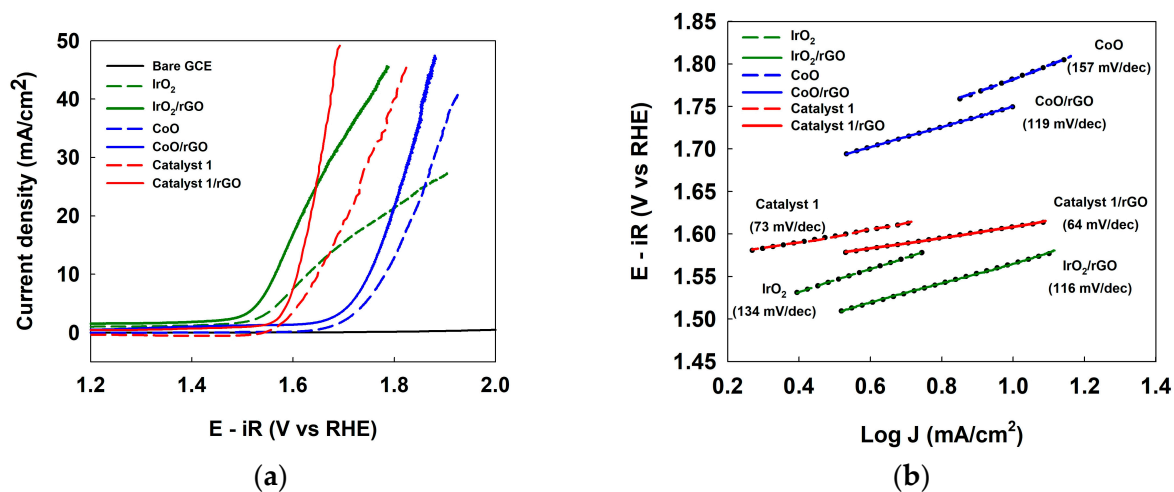


**Figure 2.** (a) Linear sweep voltammetry (LSV) and (b) Tafel plots of bare (black solid) glassy carbon electrodes (GCEs), catalyst 1/rGO composite- (red solid), catalyst 1-(red dashed), CoO/rGO composite-(blue solid), CoO-(blue dashed), IrO<sub>2</sub>/rGO composite-(green solid), and IrO<sub>2</sub>-(green dashed) modified GCE in the OER. The electrolyte solution was O<sub>2</sub>-saturated 0.1 M KOH. A scan rate of 100 mV/s and a rotation rate of 1600 rpm were used for the rotating disk electrode (RDE). All potentials were reported after the IR compensation.

The overpotentials ( $V_j$ ) at a current density of 10 mA cm<sup>-2</sup> for catalyst 1, CoO, and IrO<sub>2</sub> with the rGO-modified GCEs were 386, 526, and 341 mV, respectively (Table 1). The overpotential of the catalyst 1/rGO composite was much lower than that of CoO but slightly higher than that of the noble metal catalysts, such as IrO<sub>2</sub>.

**Table 1.** Overpotential and Tafel slope of the electrocatalysts.

Catalyst	$V_J$ (V at $J = 10 \text{ mA cm}_{\text{geo}}^{-2}$ ) <sup>1</sup>	Tafel Slope ( $\text{mV dec}^{-1}$ )
Catalyst 1/rGO	386 mV	64
Catalyst 1	426 mV	73
CoO/rGO	526 mV	119
CoO	558 mV	157
IrO <sub>2</sub> /rGO	341 mV	116
IrO <sub>2</sub>	405 mV	134

<sup>1</sup> The geometric area of the electrode, which was  $0.196 \text{ cm}^2$ , was used for the calculations.

The kinetic parameters, including the Tafel slope, were also investigated, as shown in Figure 2b. [23] The Tafel slopes of the catalyst 1/rGO composite- and catalyst 1-modified GCEs were 64 and 73  $\text{mV/dec}$ , respectively (Table 1). The small Tafel slope of the catalyst 1/rGO composite indicated the best kinetic performance compared to the reference materials. The Tafel slopes of the reference electrocatalysts, which included CoO and IrO<sub>2</sub> with or without rGO, were 119, 157, 116, and 134  $\text{mV/dec}$ , respectively.

Surprisingly, the small onset potential and Tafel slope values of the catalyst 1/rGO composite mean that it exhibits excellent electrocatalytic activity toward OERs from both thermodynamic and kinetic perspectives. The catalyst 1/rGO composite outperformed or was comparable to catalyst 1 alone or other metal oxide reference materials, such as CoO and IrO<sub>2</sub>, with or without rGO supports.

To test the durability of the electrocatalyst, long-time chronoamperometry (CA) was conducted for the catalyst 1/rGO composite. The CA experiments were performed with an applied potential, where the expected current density was  $10 \text{ mA cm}^{-2}$ . As shown in Figure 3, the current density of the catalyst 1-modified GCE was maintained at  $\geq 90\%$  for 12 h. However, the current density of the catalyst 1/rGO composite-modified GCE was maintained at  $\geq 64\%$  for 12 h, which was worse than that of catalyst 1 alone. According to the X-ray photoelectron spectroscopy (XPS) analysis, which will be described in the next section, there are no significant structural changes between the samples with/without rGO and before/after the electrochemical treatments. Therefore, these results suggested that the interaction between catalyst 1 and the electrode was stronger than the one between the catalyst 1/rGO complex and the electrode; thus, this settlement could be maintained even during vigorous gas evolution reactions.

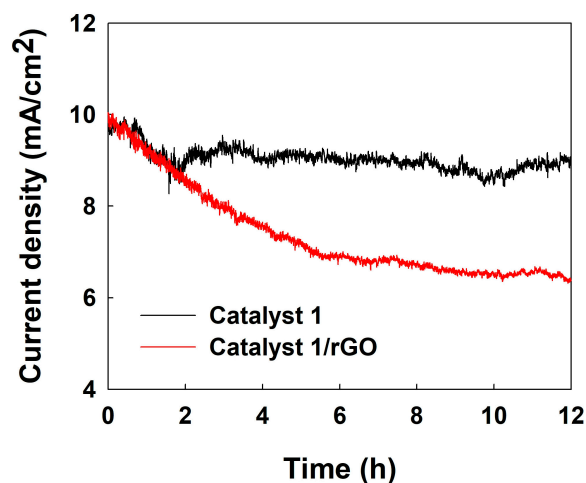


**Figure 3.** Chronoamperograms of the catalyst 1/rGO composite- (red) and catalyst 1-modified (black) GCEs during the OER. The electrolyte solution was O<sub>2</sub>-saturated 0.1 M KOH. The rotation rate of RDE was 1600 rpm.

### 3. Discussion

Recently, we reported a highly active new OER electrocatalyst, cobalt cinnamate,  $[\text{Co}_7(\text{trans-cinnamate})_{14}(\text{H}_2\text{O})_2]$ , in which the  $\pi$ - $\pi$  orbital delocalization of the *trans*-cinnamate ligand allowed for fast charge transfer through the 3D structure, followed by electron flexibility near the metal center, which improved the OER activity [14,19–21]. Pyridine ligands may have a template effect on the formation of the skeletal structure, depending on the size and shape of the amine used, and may have various levels of structural diversity when used as ligands. Therefore, the addition of a pyridine ligand during the formation of coordination polymers, including MOFs, is expected to bring various structural changes while maintaining electrocatalytic properties.

In this study, a new cobalt complex, abbreviated as **1**, was prepared by using *trans*-cinnamate and 2-aminopyrimidine ligands. In compound **1**, the  $\pi$ - $\pi$  orbital delocalization was modulated compared to cobalt cinnamate,  $[\text{Co}_7(\text{trans-cinnamate})_{14}(\text{H}_2\text{O})_2]$ , by introducing 2-aminopyrimidine ligands. The 2-aminopyrimidine ligand is also stabilized by the  $\pi$ - $\pi$  orbital delocalization. Although the comparison of electrical effects between the two ligands is indirect, considering that pure nitrogen is a better electron-donating element than oxygen, it is predicted that the nitrogen of 2-aminopyrimidine can have a rather strong metal–nitrogen bond compared to the oxygen of *trans*-cinnamate. This Co coordination environment of **1** in electron-rich environments was somewhat disadvantageous compared to that of cobalt cinnamate. Therefore, catalyst **1** may show relatively lower activity than the previously reported cobalt cinnamate (with or without rGO with a  $V_j$  of 327 and 358 mV, respectively) [15]. In spite of that, catalyst **1** is still a good electrocatalyst for OERs compared to  $\text{IrO}_2$ , as shown in Figures 4 and 5.

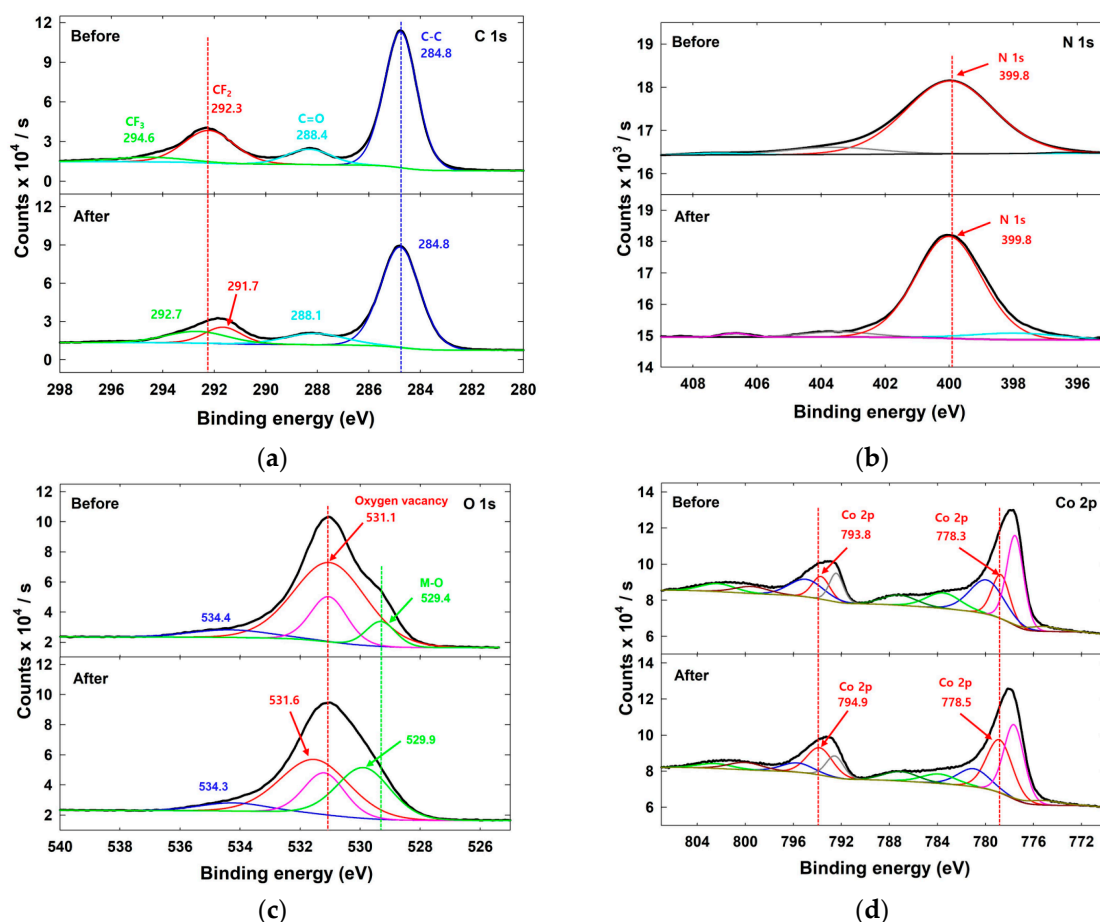


**Figure 4.** XPS spectra for (a) C 1s, (b) N 1s, (c) O 1s, and (d) Co 2p regions using a catalyst **1**/rGO composite-modified indium tin oxide (ITO) electrode before and after electrochemical measurements. The colored lines show the result of deconvolution.

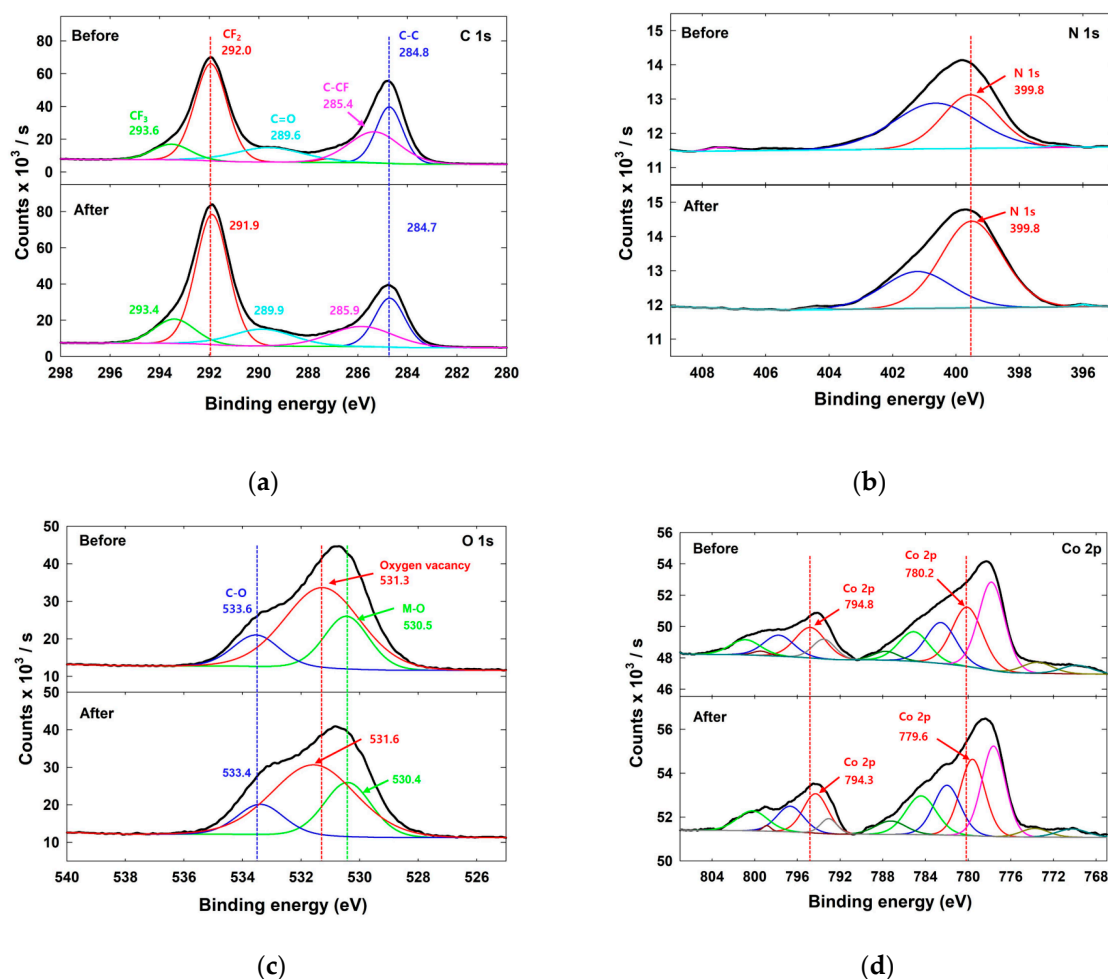


**Figure 5.** XPS spectra for (a) C 1s, (b) N 1s, (c) O 1s, and (d) Co 2p regions using a catalyst 1-modified ITO electrode before and after electrochemical measurements. The colored lines show the result of deconvolution.

In addition, the rGO supporter, which is a widely used carbon-based supporter, was introduced to reinforce the effectiveness of insufficient  $\pi$ - $\pi$  stacking interactions and increase stability. As a result of the participation of the rGO supporter, the onset potential was improved, as shown in Figure 2. The reduced overpotential with the rGO supporter seemed to be due to a strong interaction between the catalyst 1 and rGO, such as additional  $\pi$ - $\pi$  stacking interactions between the ligand and rGO. On the other hand, a reduction in the overpotential was also seen in the CoO/rGO and IrO<sub>2</sub>/rGO composites. This was thought to be because the mixing of rGO increased the electrical conductivity of CoO or IrO<sub>2</sub> on the electrode surface.

As shown in Figure 3, the catalyst 1/rGO composite has relatively low stability compared to the excellent stability of catalyst 1 because the interaction between catalyst 1 and the electrode is stronger than the interaction between the rGO and the electrode.

To identify the enhanced electrocatalytic activity based on the electronic structure modulation of the catalysts, X-ray photoelectron spectroscopy (XPS) analyses before and after the OER measurements were performed. Figures 4 and 5 show the XPS spectra for C, N, O, and Co of catalyst 1 with or without an rGO supporter.

As shown in Figures 4 and 5, the main C 1s peaks were obtained at ~284.8 eV (blue line) in the catalyst 1/rGO composite and at ~292.0 eV (red line) in catalyst 1 alone. Since the peak at 284.8 eV represents C in highly oriented pyrolytic graphite (HOPG) [24], this seems to be due to the rGO supporter. The peaks at 292.0 eV represent C connected to highly electronegative atoms (e.g., CF<sub>2</sub>, CO<sub>3</sub><sup>2-</sup>) [24], which seems to be due to the

Nafion and cinnamate parts. Therefore, the increment of peak size (counts) in the whole binding energy region and the shift in the main peak from 292.0 to 284.8 eV indicated the successive introduction of the rGO supporter into the catalyst. [15] However, there was no significant change in the position or size of the peaks before and after the electrochemical measurements. For N, O, Co, and C, there were few differences in the chemical states before and after the electrochemical measurements.

For N, the main N 1s peaks were obtained at ~399.8 eV in both cases and before/after the electrochemical measurements, which seemed to correspond to the N 1s peak at ~398.3 eV, as mentioned in the literature [25]. The N 1s peaks were not significantly shifted after the composite formation.

The O 1s peaks were observed at ~529.4 (green line) and ~531.1 eV (red line), representing the lattice oxygen and oxygen vacancy (defect), respectively [26,27]. For catalyst **1**, the strongest peak corresponding to the oxygen vacancy (at ~531.1 eV) was still retained after the rGO composite formation. The existence of a large area of the peak at ~531.1 eV implied the existence of oxygen vacancies and a high electrocatalytic activity of the composite and catalyst **1** [26]. In the case of catalyst **1** alone, the small peak at ~533.4 eV that appeared more prominent indicated that a different oxidation state of oxygen was available.

The Co 2p peaks of catalyst **1** were observed at ~780.2 and ~794.8 eV with small satellite peaks before and after the electrochemical measurements. For the catalyst **1**/rGO composite, the Co 2p peaks appeared at a lower binding energy region, between ~778.3 and ~793.8 eV, than that of catalyst **1**, which revealed the electronic interaction between the catalyst and rGO [28].

Therefore, the XPS analyses suggested that catalyst **1** has enhanced oxygen vacancies and a more exposed Co center, which can improve the electrocatalytic activity toward OERs.

## 4. Materials and Methods

### 4.1. Reagents

Cobalt (II) chloride hexahydrate (99.9%) was purchased from Alfa Aesar (Haverhill, MA, USA). Aldrich supplied the 2-aminopyrimidine (97%) reagent (St. Louis, MO, USA), and *trans*-cinnamic acid (99+%) was obtained from Acros Organics (Geel, Antwerp, Belgium). All chemicals were used as received.

### 4.2. Preparation of Electrocatalyst

The catalysts were synthesized by mixing cobalt (II) chloride hexahydrate (0.284 g, 1.2 mmol), 2-aminopyrimidine (0.348 g, 3.6 mmol), *trans*-cinnamic acid (0.088 g, 0.6 mmol), and distilled water (1.0 mL). The obtained solution was sealed in a Pyrex<sup>®</sup> tube, heated to 100 °C for 68 h, and finally cooled to room temperature at a rate of 20 °C/h. The pH of the solution before and after the reaction was ~4 and ~7, respectively. The solid products were recovered from the solution by employing vacuum filtration and then washed with ethanol. Red polyhedral-shaped crystals of  $\text{Co}_2(\text{trans-cinnamate})_4(2\text{-aminopyrimidine})_2(\text{H}_2\text{O}) \cdot 2.5\text{H}_2\text{O}$  (referred to as **1**) and unidentified pink ribbon-shaped crystals were obtained. Due to their large size, the two types of solid products were manually separated using a microscope (~millimeter scale). Energy-dispersive X-ray spectroscopy (EDS) analyses confirmed the presence of Co in **1**. For **1**: elemental analysis (%) calculated: C 58.78, H 7.59, N 10.55, and O 12.05; found: C 56.83, H 7.15, N 9.98, and O 11.80. IR(KBr): 3315 s, 3285 s, 3174 m, 3061 w, 3022 w, 2958 m, 2927 m, 2858 m, 1637 m, 1597 m, 1538 s, 1462 m, 1445 m, 1434 m, 1380 s, 1338 m, 1306 w, 1263 w, 1207 w, 1139 s, 1039 w, 1073 w, 1207 s, 1002 w, 984 m, 926 m, 895 s, 862 m, 815 w, 779 s, 745 w, 707 m, 688 m, 674 m, 634 m, 590 m, 555 m, 521 m, and 500  $\text{m cm}^{-1}$ .

### 4.3. Single Crystal Structure Determinations

The single-crystal X-ray analysis was performed using a Siemens SMART diffractometer (Siemens AG, Munich, Germany) outfitted with an Apex II area detector and a graphite-monochromatized Mo K $\alpha$  radiation. The structures were determined by employing direct methods and then refined by SHELXS and ShelXle with the SHELXL plug-in [29–31]. The

hydrogen atoms of *trans*-cinnamate and 2-aminopyrimidine were generated geometrically and allowed to ride on their respective parent atoms. The oxygen atoms of the lattice water molecules were refined isotopically owing to their heavily disordered behavior and low occupancy. All crystal data are summarized in Table S1. The Cambridge Crystallographic Data Center (CCDC) reference number for 1 is 2232776. The data can be obtained free of charge from the CCDC. The crystallographic details, atomic coordinates, selected bond distances, and angles are given in Tables S1–S3.

#### 4.4. Electrochemical Characterization

A glassy carbon electrode (GCE) (with a diameter of 5 mm; Pine Research Instrumentation, Durham, NC, USA) was used as a support for the catalysts. The loading sample solution with a concentration of 2 mg/mL was prepared by dissolving each powder of 1, IrO<sub>2</sub>, and CoO in an ethanol/water (1:1 *v/v*) solution. In both cases, 20 μL of Nafion was added and ultrasonicated for 30 min. Finally, 7 μL of the loading sample solution was dropped onto the cleaned GCE and dried for 1 d.

A three-electrode cell consisting of a Pt wire counter electrode, a catalyst-modified GCE, and an Ag/AgCl (1 M KCl; 0.235 V vs. NHE) reference electrode were used for the electrochemical experiments. The electrolyte solution for the OER was O<sub>2</sub>-saturated 0.1 M KOH, and its solution resistance obtained from the conductivity measurement was ~42 Ω. The 100 % IR-compensated potentials were reported vs. the reversible hydrogen electrode (RHE) and calculated using the following equation:

$$\text{RHE} = E (\text{vs. Ag/AgCl}) + 0.059 \times \text{pH} + 0.235 \text{ V}$$

#### 4.5. Instruments

The powder X-ray diffraction (XRD) analyses were performed using a Rigaku Ultra X-ray diffractometer (Applied Rigaku Technologies, Austin, TX, USA) equipped with Cu Kα radiation. The infrared spectra (IR) were recorded using the KBr pellet method on a Nicolet 6700 FT-IR spectrometer (Thermo Fisher Scientific, Waltham, MA, USA) in the range of 400–4000 cm<sup>-1</sup>. The XPS was measured using a Thermo Scientific K-Alpha X-ray photoelectron spectrometer (Waltham, MA, USA). The samples were drop-casted onto an indium tin oxide (ITO) electrode for the electrochemical treatments. The elemental analyses of 1 were performed at Sogang University. All electrochemical measurements with the rotating disk electrode (RDE) were performed using a CHI model 750d potentiostat (CH Instruments, Austin, TX, USA) and an RRDE-3A (ALS Co., Ltd., Tokyo, Japan).

## 5. Conclusions

We demonstrated the electrocatalytic activity of a new 1D cobalt cinnamate complex consisting of 2-aminopyrimidine with/without an rGO supporter for OERs. The unique tetrameric Co<sub>4</sub> units consisting of π-conjugated *trans*-cinnamate and 2-aminopyrimidine were expected to exhibit similar electrochemical activities. Similar to the *trans*-cinnamate anion, the molecular 2-aminopyrimidine ligand exhibits a π–π delocalized structure, which appears to have an effect on the formation of a Co–O/N environment, which is crucial for catalytic activity. Therefore, the electronic structure modulation of Co by effective electron conjugation with both *trans*-cinnamate and 2-aminopyrimidine ligands could provide a great electrocatalytic behavior with a small overpotential and Tafel slope. In addition, the improvement of the electrocatalytic properties of the composite was due to the feasible chemical interactions between the rGO supporter and the π-conjugated groups of the ligand. Exploring new metal complexes by introducing various π–π delocalized organic ligands could provide a new direction for improving electrocatalytic activity. In future studies, it will be possible to improve the electrocatalytic activity of the catalyst by controlling the three-dimensional structure or the electronic structure modulation of its metal center through the introduction of a ligand derivative and central metal substitution.

## 6. Patents

This section is not mandatory; however, it may be added if there are patents resulting from the work reported in this manuscript.

**Supplementary Materials:** The following supporting information can be downloaded at: <https://www.mdpi.com/article/10.3390/catal13030507/s1>, Tables S1–S3: Crystal data and structure refinement details, atomic coordinates, and selected bond lengths and angles for **1**; Figure S1: Powder XRD pattern of **1**; Figure S2: IR of **1**.

**Author Contributions:** Conceptualization, S.J.K. and J.D.; methodology, J.L. and H.S.; investigation, J.L., H.S., S.G. and S.L.; data curation, K.M.O.; writing—original draft preparation, J.D. and S.J.K.; writing—review and editing, J.D. and S.J.K.; supervision, J.D. and S.J.K. All authors have read and agreed to the published version of the manuscript.

**Funding:** This research was supported by the National Research Foundation of Korea (NRF) grant funded by the Korean government (MSIT) (2021R1A2C1013995, 2021R1F1A1060277).

**Conflicts of Interest:** The authors declare no conflict of interest.

## References

1. Wang, Y.; Chen, K.S.; Mishler, J.; Cho, S.C.; Adroher, X.C. A review of polymer electrolyte membrane fuel cells: Technology, applications, and needs on fundamental research. *Appl. Energy* **2011**, *88*, 981–1007. [CrossRef]
2. Chu, S.; Majumdar, A. Opportunities and challenges for a sustainable energy future. *Nature* **2012**, *488*, 294–303. [CrossRef] [PubMed]
3. Fillol, J.L.; Codolà, Z.; Garcia-Bosch, I.; Gómez, L.; Pla, J.J.; Costas, M. Efficient water oxidation catalysts based on readily available iron coordination complexes. *Nat. Chem.* **2011**, *3*, 807–813. [CrossRef]
4. Bai, Y.; Liu, C.; Shan, Y.; Chen, T.; Chen, T.; Zhao, Y.; Yu, C.; Pang, H. Metal-organic frameworks nanocomposites with different dimensionalities for energy conversion and storage. *Adv. Energy Mater.* **2021**, *12*, 2100346. [CrossRef]
5. Li, X.; Yang, X.; Xue, H.; Pang, H. Metal-organic frameworks as a platform for clean energy applications. *EnergyChem* **2020**, *2*, 100027. [CrossRef]
6. Oh, S.H.; Black, R.; Pomerantseva, E.; Lee, J.-H.; Nazar, L.F. Synthesis of a metallic mesoporous pyrochlore as a catalyst for lithium–O<sub>2</sub> batteries. *Nat. Chem.* **2012**, *4*, 1004–1010. [CrossRef]
7. Li, Y.; Zhang, X.; Zheng, Z. A review of transition metal oxygen-evolving catalysts decorated by cerium-based materials: Current status and future prospects. *CCS Chem.* **2022**, *4*, 31–53. [CrossRef]
8. Reier, T.; Oezaslan, M.; Strasser, P. Electrocatalytic oxygen evolution reaction (OER) on Ru, Ir, and Pt catalysts: A comparative study of nanoparticles and bulk materials. *ACS Catal.* **2012**, *2*, 1765–1772. [CrossRef]
9. Lee, Y.; Suntivich, J.; May, K.J.; Perry, E.E.; Shao-Horn, Y. Synthesis and activities of rutile IrO<sub>2</sub> and RuO<sub>2</sub> nanoparticles for oxygen evolution in acid and alkaline solutions. *J. Phys. Chem. Lett.* **2012**, *3*, 399–404. [CrossRef] [PubMed]
10. Subbaraman, R.; Tripkovic, D.; Chang, K.-C.; Strmcnik, D.; Paulikas, A.P.; Hirunsit, P.; Chan, M.; Greeley, J.; Stamenkovic, V.; Markovic, N.M. Trends in activity for the water electrolyser reactions on 3d M(Ni,Co,Fe,Mn) hydr(oxy)oxide catalysts. *Nat. Mater.* **2012**, *11*, 550–557. [CrossRef] [PubMed]
11. Han, L.; Dong, S.; Wang, E. Transition-Metal (Co, Ni, and Fe)-Based Electrocatalysts for the Water Oxidation Reaction. *Adv. Mater.* **2016**, *28*, 9266–9291. [CrossRef]
12. Li, S.-L.; Xu, Q. Metal-Organic frameworks as platforms for clean energy. *Energy Environ. Sci.* **2013**, *6*, 1656–1683. [CrossRef]
13. Jiao, L.; Wang, Y.; Jiang, H.; Xu, Q. Metal-organic frameworks as platforms for catalytic applications. *Adv. Mater.* **2018**, *30*, 1703663–1703685. [CrossRef]
14. Kang, J.; Lee, M.J.; Oh, N.G.; Shin, J.; Kwon, S.J.; Chun, H.; Kim, S.-J.; Yun, H.; Jo, H.; Ok, K.M.; et al. I<sup>3</sup>O<sup>0</sup>-type 3D framework of cobalt cinnamate and its efficient electrocatalytic activity toward oxygen evolution reaction. *Chem. Mater.* **2021**, *33*, 2804–2813. [CrossRef]
15. Lee, M.J.; Kim, J.; Kang, J.; Shin, H.; Do, J.; Kwon, S.J. Electrocatalytic Activity of Reduced Graphene Oxide Supported Cobalt Cinnamate for Oxygen Evolution Reaction. *Energies* **2021**, *14*, 5020. [CrossRef]
16. He, D.; Song, X.; Li, W.; Tang, C.; Liu, J.; Ke, Z.; Jiang, C.; Xiao, X. Active Electron Density Modulation of Co<sub>3</sub>O<sub>4</sub>-Based Catalysts Enhances their Oxygen Evolution Performance. *Angew. Chem. Int. Ed.* **2020**, *59*, 6929–6935. [CrossRef] [PubMed]
17. Si Liu, S.; Lei, Y.-J.; Xin, Z.-J.; Xiang, R.-J.; Styring, S.; Thapper, A.; Wang, H.-Y. Ligand modification to stabilize the cobalt complexes for water oxidation. *Int. J. Hydrog. Energy* **2017**, *42*, 29716–29724. [CrossRef]
18. Treadway, J.A.; Loeb, B.; Lopez, R.; Anderson, P.A.; Keene, F.R.; Meyer, T.J. Effect of delocalization and rigidity in the acceptor ligand on MLCT excited-state decay. *Inorg. Chem.* **1996**, *35*, 2242–2246. [CrossRef]
19. Yun, S.; Lee, S.; Shin, C.; Park, S.; Kwon, S.J.; Park, H.S. One-pot self-assembled, reduced graphene oxide/palladium nanoparticle hybrid aerogels for electrocatalytic applications. *Electrochim. Acta* **2015**, *180*, 902–908. [CrossRef]
20. Huang, X.; Qi, X.; Boey, F.; Zhang, H. Graphene-based composites. *Chem. Soc. Rev.* **2012**, *41*, 666–686. [CrossRef] [PubMed]

21. Abidat, I.; Cazayus, E.; Loupiau, L.; Morais, C.; Comminges, C.; Napporn, T.W.; Portehault, D.; Durupthy, O.; Mamede, A.-S.; Chanéac, C.; et al.  $\text{Co}_3\text{O}_4/\text{rGO}$  catalysts for oxygen electrocatalysis: On the role of the oxide/carbon interaction. *J. Electrochem. Soc.* **2019**, *166*, H94–H102. [[CrossRef](#)]
22. Brese, N.E.; O’Keeffe, M. Bond-valence parameters for solids. *Acta Crystallogr.* **1991**, *47*, 192–197. [[CrossRef](#)]
23. Bard, A.J.; Faulkner, L.R. *Electrochemical Methods: Fundamentals and Applications*, 2nd ed.; John Wiley & Sons: New York, NY, USA, 2001.
24. Al-Gaashani, R.; Najjar, A.; Zakaria, Y.; Mansour, S.; Atieh, M.A. XPS and structural studies of high quality graphene oxide and reduced graphene oxide prepared by different chemical oxidation methods. *Ceram. Int.* **2019**, *45*, 14439–14448. [[CrossRef](#)]
25. Crist, B.V. *Handbook of Monochromatic XPS Spectra: The Elements of Native Oxides*; XPS International, Inc.: Mountain View, CA, USA, 1999.
26. Meng, C.; Lin, M.; Sun, X.; Chen, X.D.; Chen, X.M.; Du, X.; Zhou, Y. Laser synthesis of oxygen vacancy-modified  $\text{CoOOH}$  for highly efficient oxygen evolution. *Chem. Commun.* **2019**, *55*, 2904–2907. [[CrossRef](#)]
27. Xu, W.; Lyu, F.; Bai, Y.; Gao, A.; Feng, J.; Cai, Z.; Yin, Y. Porous cobalt oxide nanoplates enriched with oxygen vacancies for oxygen evolution reaction. *Nano Energy* **2018**, *43*, 110–116. [[CrossRef](#)]
28. Pan, S.; Mao, X.; Yu, J.; Hao, L.; Du, A.; Li, B. Remarkably improved oxygen evolution reaction activity of cobalt oxides by an Fe ion solution immersion process. *Inorg. Chem. Front.* **2020**, *7*, 3327–3339. [[CrossRef](#)]
29. Sheldrick, G.M. A short history of SHELX. *Acta Crystallogr.* **2008**, *64*, 112–122. [[CrossRef](#)]
30. Spek, A.L. Structure validation in chemical crystallography. *Acta Crystallogr.* **2009**, *65*, 148–155. [[CrossRef](#)] [[PubMed](#)]
31. Sheldrick, G.M. SHELXT—Integrated space-group and crystal-structure determination. *Acta Crystallogr.* **2015**, *71*, 3–8. [[CrossRef](#)]

**Disclaimer/Publisher’s Note:** The statements, opinions and data contained in all publications are solely those of the individual author(s) and contributor(s) and not of MDPI and/or the editor(s). MDPI and/or the editor(s) disclaim responsibility for any injury to people or property resulting from any ideas, methods, instructions or products referred to in the content.